



HAL
open science

Microstructural evolution during the crack propagation at the bond-wire contact area of IGBT power modules upon power cycling

Mustafa Shqair, Zoubir Khatir, Ali Ibrahim, Ayda Halouani, Mounira Bouarroudj-Berkani

► To cite this version:

Mustafa Shqair, Zoubir Khatir, Ali Ibrahim, Ayda Halouani, Mounira Bouarroudj-Berkani. Microstructural evolution during the crack propagation at the bond-wire contact area of IGBT power modules upon power cycling. *Microelectronics Reliability*, 2022, 10.1016/j.microrel.2022.114635 . hal-03788643

HAL Id: hal-03788643

<https://hal.science/hal-03788643>

Submitted on 26 Sep 2022

HAL is a multi-disciplinary open access archive for the deposit and dissemination of scientific research documents, whether they are published or not. The documents may come from teaching and research institutions in France or abroad, or from public or private research centers.

L'archive ouverte pluridisciplinaire **HAL**, est destinée au dépôt et à la diffusion de documents scientifiques de niveau recherche, publiés ou non, émanant des établissements d'enseignement et de recherche français ou étrangers, des laboratoires publics ou privés.



HAL
open science

Microstructural evolution during the crack propagation at the bond-wire contact area of IGBT power modules upon power cycling

Mustafa Shqair, Zoubir Khatir, Ali Ibrahim, Ayda Halouani, Mounira Berkani

► To cite this version:

Mustafa Shqair, Zoubir Khatir, Ali Ibrahim, Ayda Halouani, Mounira Berkani. Microstructural evolution during the crack propagation at the bond-wire contact area of IGBT power modules upon power cycling. *Microelectronics Reliability*, Elsevier, 2022, pp.114635. 10.1016/j.microrel.2022.114635 . hal-03788643

HAL Id: hal-03788643

<https://hal.archives-ouvertes.fr/hal-03788643>

Submitted on 26 Sep 2022

HAL is a multi-disciplinary open access archive for the deposit and dissemination of scientific research documents, whether they are published or not. The documents may come from teaching and research institutions in France or abroad, or from public or private research centers.

L'archive ouverte pluridisciplinaire **HAL**, est destinée au dépôt et à la diffusion de documents scientifiques de niveau recherche, publiés ou non, émanant des établissements d'enseignement et de recherche français ou étrangers, des laboratoires publics ou privés.

Microstructural evolution during the crack propagation at the bond-wire contact area of IGBT power modules upon power cycling

Mustafa Shqair^{a,*}, Zoubir Khatir^a, Ali Ibrahim^a, Ayda Halouani^a, Mounira Berkani^b

^a Gustave Eiffel University, Paris-Saclay Univ., ENS Paris-Saclay, CNRS, SATIE, 78000 Versailles, France

^b Paris Est Créteil University, Paris-Saclay Univ., CNRS, SATIE, 91190 Gif-Sur-Yvette, France

ARTICLE INFO

Keywords:

IGBT
Metallic contacts
Microstructure
Crack
Grains size
Disorientation angles
Grains texture

ABSTRACT

This paper proposes an analysis for the main microstructural changes at the chip topside level in the metallic interconnections of SKIM63 IGBT power modules due to aging processes caused by power cycling. The objective is to correlate these changes with the degradation processes dominating such positions. In this study, it is deduced that grains stability drives their texture evolution upon cycling. Transformations of texture components, which indicate whether the structure is recrystallized or deformed, are analyzed at different cycling stages. Afterward, the effect of the evolution of the disorientation angle's distribution on the crack passage is discussed. The size of grains directly related to their strength was as well shown to affect the cracking manner. Finally, the cracking procedure is interpreted in detail.

1. Introduction

IGBT devices are widely used in electronic applications due to their ability to converge high current loads with high efficiency and speed. Thermomechanical fatigue of topside metallic contacts in power devices such as IGBTs is one of the critical reliability issues. It results from the existence of different materials having different thermal expansion coefficients, mainly aluminum (Al) composing metallization chips and ultrasonically bonded wires, and silicon (Si) which lays beneath them. Thermomechanical fatigue causes major degradations at the metallic contact sites since deformations are maximal there.

Because grain reconstructions and crack propagation are synchronous during degradation processes, the analysis of their evolution is of high importance. Grain reconstructions lead to several changes in material properties. The crack propagation is responsible for the failure of top metallic parts in power modules. This may signify a relationship between both crack propagation and reconstruction processes [1–4]. Thus, several microstructural features were analyzed in this paper and then related to the cracking manner. Accelerated power cycling tests were applied on SKIM63 IGBT samples manufactured by Semikron at different cycling stages [5,6]. Microstructural analyses have been performed using Electron backscattered diffraction (EBSD) technique. The zone of interest for analyzing these microstructural properties is selected through partitioning the EBSD data using the ATEX program [7]. These

analyses enable us to understand what happens microstructurally in a SKIM63 IGBT module at the wire-metallization contact when degradations occur. This study can also be used as a basis for constructing a crack formation model at the wire-metallization interconnection.

2. Methodology

Aging tests under the following conditions {Junction temperature rise (ΔT_j) = 110 °C, minimal junction temperature ($T_{j,min}$) = 55 °C, power-on duration (t_{on}) = 3 s, power-off duration (t_{off}) = 6 s} were applied on several half-bridge (mid leg) SKIM63 substrates, and removed from the test bench at different aging stages [5]. It was deduced that the crack propagation manner is reproducible on all the wires. Thus, it was assumed that microstructural degradation processes are identical too. Far-right wires of central chips were analyzed by EBSD. The following numbering of the chips given in Fig. 1 will be considered in the upcoming analyses.

3. Microstructural analysis

Fig. 2 shows an example of the crack propagation evolution at the chip topside, i.e., bond-wire contacts.

The crack propagates in the wire just above the metallization in accordance with the literature [8]. Consequently, only this wire zone is

* Corresponding author.

E-mail address: mustafa.shqair@univ-eiffel.fr (M. Shqair).

<https://doi.org/10.1016/j.microrel.2022.114635>

Received 3 June 2022; Received in revised form 8 July 2022; Accepted 10 July 2022

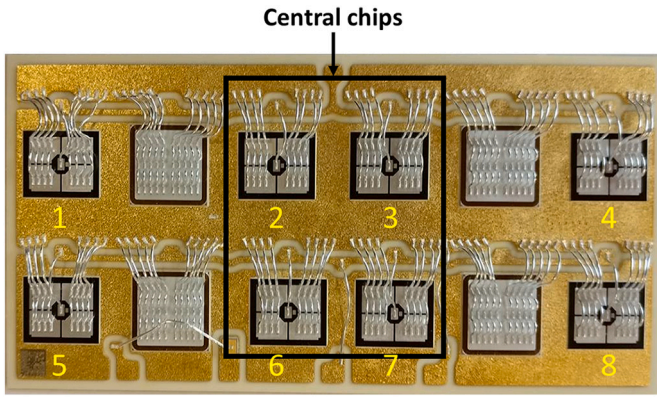


Fig. 1. One half-bridge substrate of a SKIM63 module.

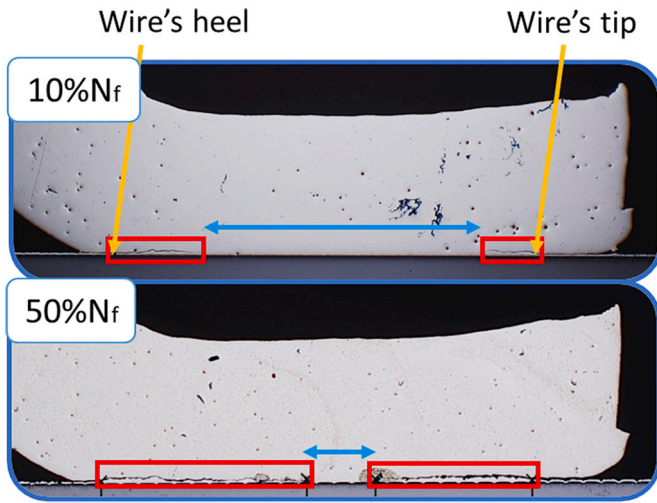


Fig. 2. Cracks evolution at the upper metallic interface.

considered in this study. It was deduced that the initial crack speed is clearly higher than that for its propagation at advanced cycling stages, with a faster speed at the heel position. EBSD plots were partitioned in two ways to interpret the microstructural changes at the wire's contact zone, the first one at the entire wire contact area and the second at the wire's edges.

3.1. The first partitioning analysis

A first partitioning as observed in Fig. 3 inside the wire just above the metallization was made to analyze the evolution of grains texture, and see the effect of grains size and disorientation angles on the cracking process. This was applied for two wires samples in chips #2 and #6 of

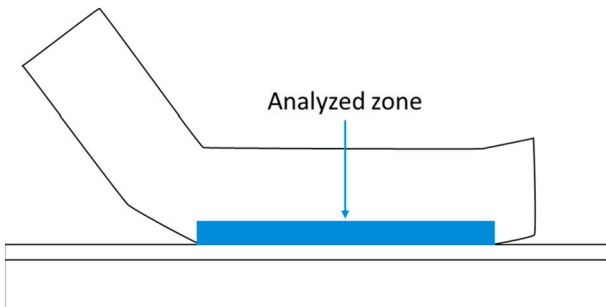


Fig. 3. The first partitioned zone.

different substrates aged at different cycling stages. The microstructural evolutions resulting in both samples are identical. This paper presents only evolutions in the wire of chip #2.

3.1.1. Grains texture evolution upon cycling

The driving force for reconstructions is surface energy reduction, which increases grain's stability [9]. This partitioning is primarily made to confirm that during aging. In face-centered cubic (FCC) metals such as Al, the decreasing order of packing density of crystal faces is (111), (001), and (101) [10]. The decreasing order of surface energy values of crystal faces is (101), (001), and (111) [11]. Thus, it should be noted that the less favored orientation to form is (101). Fig. 4 shows inverse pole figures (IPFs) evolution in the x-direction for a wire in chip #2 (a) before cycling and (b) cycled at 50 % N_f , where N_f corresponds to the number of cycles for the module's complete failure. For a clearer view, inverse pole images are partitioned into halves, where the upper half corresponds to the right side of the analyzed portion (from the heel edge toward the wire center), and the lower half shows the left side of the analyzed portion (from the center toward the tip edge).

Fig. 4 shows that more (111) orientation results upon cycling, accompanied by a decrease in the number of (101) orientations. This evolution confirms that grains orient to reduce the surface energy and increase the packing density.

3.1.2. Grains size & disorientation angles with cracking

The size of grains has a significant impact on their strength against cracking. According to the Hall-Petch relationship, smaller grains acquire higher strength [12]. Fig. 5 shows the grain's size number fractions evolution for a wire in chip #2 at early cycling stages (until 25 % N_f), at which the crack speed is the highest.

This size distribution in Fig. 5 shows that the grains in the analyzed area have majorly sizes $<5 \mu\text{m}$ from the beginning of cycling until reaching 25 % of N_f . However, bigger grains are formed after cycling. This is evidenced by the decrease in the number fractions of tiny grains ($<5 \mu\text{m}$), the increase in the number fractions of bigger grains (5 to 20 μm), and the generation of new grains having huge sizes ($\approx 45 \mu\text{m}$). Therefore, it is deduced that the rapid crack initiation is synchronous with grain growth.

Additionally, disorientation angles are expected to influence the formation and propagation of cracks. Fig. 6 shows the evolution of disorientation angles for the wires in chip #2 at advanced cycling stages (65–100 % N_f), at which the crack speed is decreasing. These angles are plotted beside the Mackenzie distribution, which gives the disorientation angles' distribution of a randomly oriented grain [13].

From Fig. 6, it has been reported that cracks evolution is synchronous

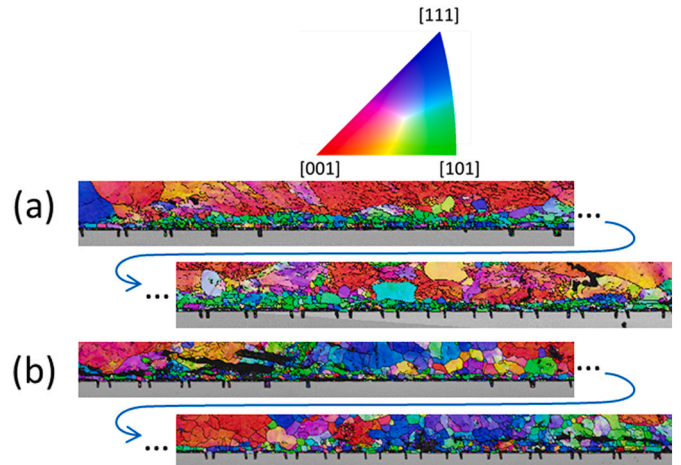


Fig. 4. Wire's texture evolution in chip #2, at (a) its healthy state and (b) cycled at 50 % N_f .

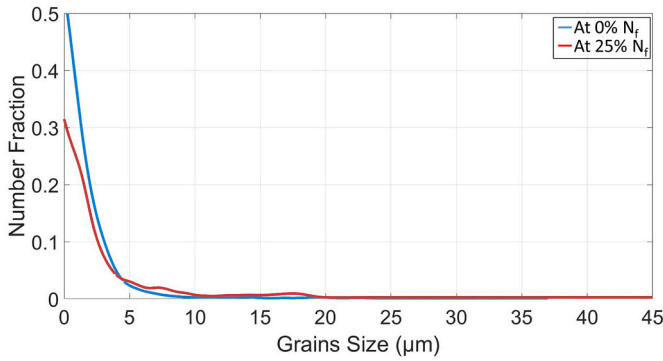


Fig. 5. The number fractions of grains size upon cycling a wire in chip #2.

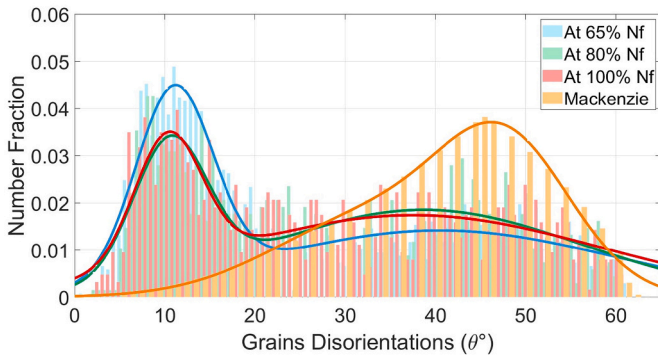


Fig. 6. The number fractions of disorientation angles upon cycling the wire in chip #2.

with the decrease in the number fractions of low angle boundaries (LABs) and the increase in that of high angle boundaries (HABs) when comparing the portion degraded at 65 % N_f with that degraded at 80 % N_f and 100 % N_f . Comparing the portions at 80 % N_f and 100 % N_f , the decrease in the number of LABs and the increase in the number of HABs are not observed. This is because cracks themselves induce deformations, especially at the lift-off moment [13,14]. The rearrangement of these deformations may cause the formation of sub-grains, which could inhibit the decrease in the number of LABs through the formation of new LABs. All these observations were also seen for the wire in chip #6.

3.2. The second partitioning analysis

A second partitioning was operated particularly at the heel and tip positions, the positions of cracks nucleation (see Fig. 2). This partitioning, as shown in Fig. 7, was done to interpret in-depth the degradation processes microstructurally. Wires in chips #6 and #7 are

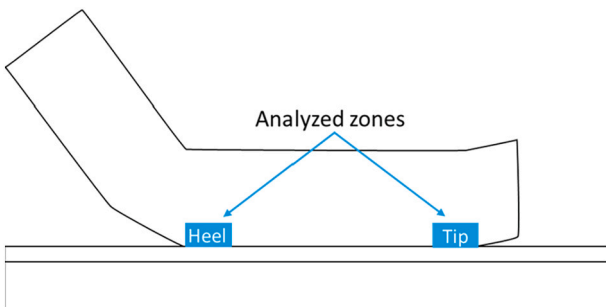


Fig. 7. The second partitioned positions.

analyzed.

Crystal texture components evolution of Al grains was analyzed during aging at both the heel and tip positions, and thus rolled FCC texture classifications are considered. Cube (Cb) and Goss (Gs) textures are associated with recrystallization [15,16], whereas Brass (Bs), Copper (Cu), Taylor (Ty), and S textures are linked to deformations [15,17,18]. The disorientation angles and grains' size evolution were analyzed as well.

For the wire in chip #6, Fig. 8 shows the evolution of texture components at the partitioned tip and heel positions during the crack initiation stages. Fig. 9 presents the disorientation angles' evolution, and Fig. 10 displays the grains' size evolution.

3.2.1. Analysis at the tip position (healthy & 10 % N_f)

Before cycling, recrystallization components are dominant at the tip, with the presence of deformation components. The wire welding forces create these components. Because big grains (representing the initial state before the wire's welding) are present beside some tiny grains, disorientation angles are randomly distributed, with high HABs frequencies.

When cycling up to 10 % N_f , recrystallization components highly increased, whereas deformation components decreased. This change is due to grains reconstructions that occur when cycling begins. Grains are majorly small due to dislocations rearrangements. The number of LABs highly increased as well. This is expected to influence the propagation of cracks at such positions. Because the crack formation is still weak at this moment, a grain growth state is expected just after 10 % N_f to cause the advanced crack propagation in the following cycling stages.

At 50 % N_f , recrystallization components lasted dominant. The volume fractions of deformation components remained shallow. This is probably because cracks are majorly formed between 10 % N_f and 50 % N_f , therefore, at 50 % N_f , cracks are already formed; thus deformations had been relieved. As predicted, grains are bigger than those at the previous cycling stage, giving a clue about grain growth. Additionally, the number fraction of LABs slightly increased, and that for HABs

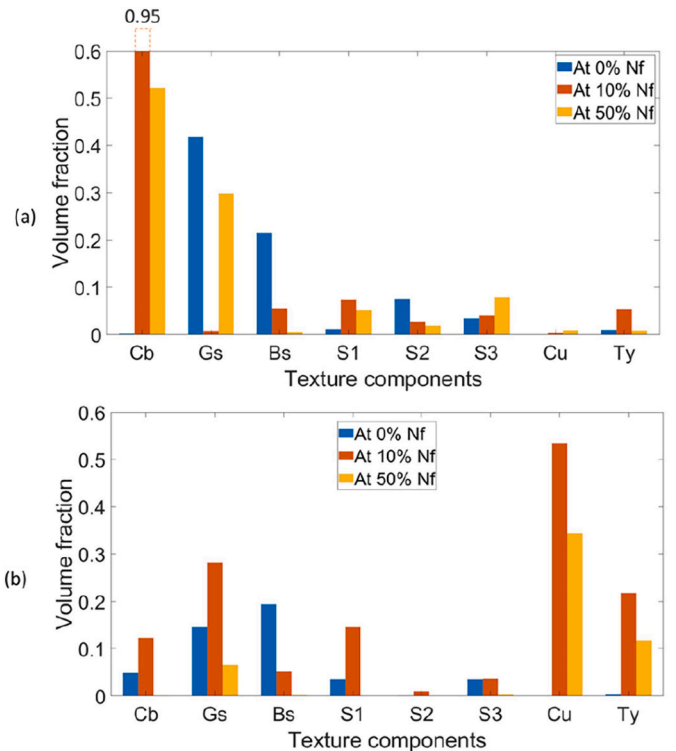


Fig. 8. Texture components' evolution in the partitioned wire positions in chip #7 at the (a) tip & (b) heel.

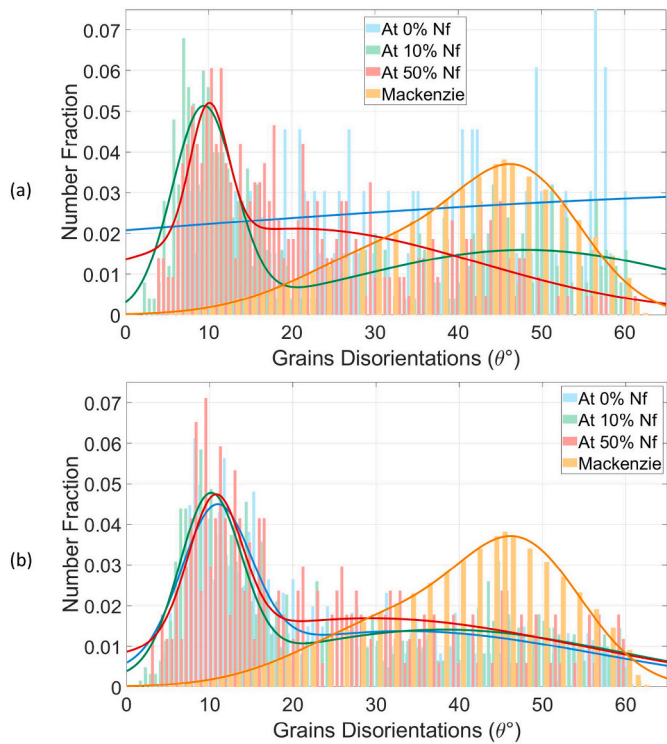


Fig. 9. Disorientation angles' evolution for the partitioned wire positions in chip #7 at the (a) tip & (b) heel.

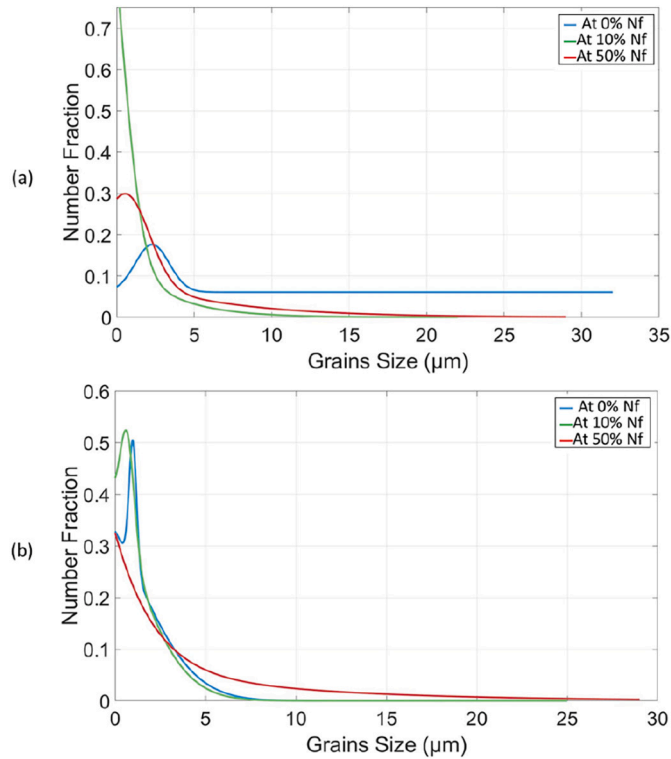


Fig. 10. Grain size's evolution for the partitioned wire positions in chip #7 at the (a) tip & (b) heel.

decreased. This evolution is synchronous with the enhanced formation of cracks at this cycling stage at the tip position.

3.2.2. Analysis at the heel position (healthy & 10 % N_f)

Initially, deformation and recrystallization components exist at the heel position due to wire welding forces, forming grains of small sizes. This may justify the dominance of LABs since grains are mostly small with close morphologies and orientations.

At 10 % N_f, deformation components increased a lot and became dominant. Such an increase is expected here, at the favored position of cracks initiation. It is deduced that the deformation component's volume fractions are higher than those at the tip. This may also signify that the heel is subjected to more deformations; consequently, the crack initiation is enhanced there. In addition, the number of LABs slightly increased, and that for HABs decreased. This happened at the same time as having a fast crack initiation. It is expected that between the healthy state and 10 % N_f, a grain growth phase occurred most probably just before 10 % N_f after recrystallization, causing the easy crack passage. This is evident from the existence of some grains with sizes between 15 and 25 μm.

When reaching 50 % N_f, even though the deformations component's volume fraction decreased, they were still dominant over recrystallization components. This dominance is logical because stress and deformations are highly formed at the heel edge. The decrease in their number fractions is probably due to the formation of cracks responsible for stress and deformations relief. Grains are clearly bigger at this cycling stage, synchronous with the significant crack progress.

In the next step, the same microstructural analysis was conducted, however at advanced cycling stages for the wire in chip #6, as seen in Figs. 11, 12, and 13.

3.2.3. Analysis at the tip position (65 % & 100 % N_f)

It has been observed that at 65 % N_f, recrystallization components dominate at the tip, with nearly null deformation components, maybe

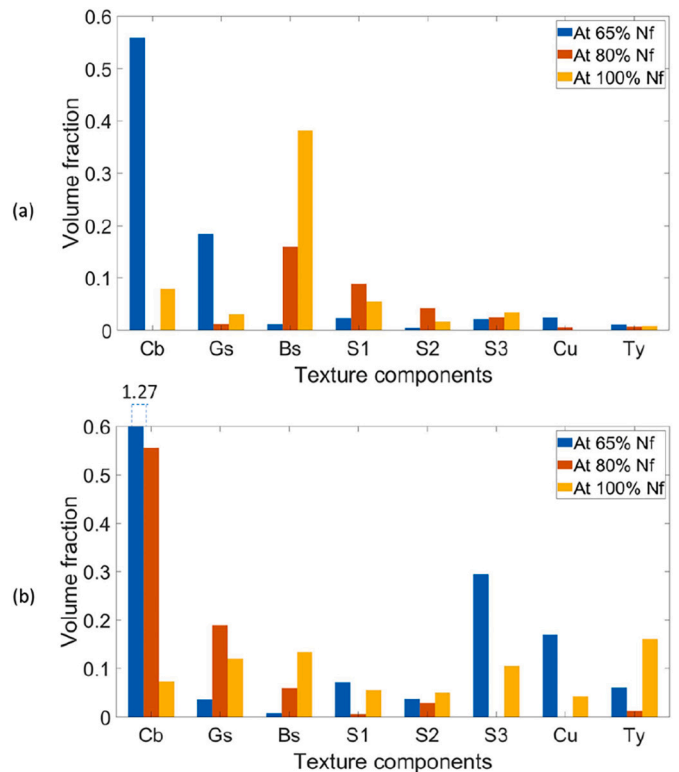


Fig. 11. Texture components' evolution in the partitioned wire positions in chip #6 at the (a) tip & (b) heel.

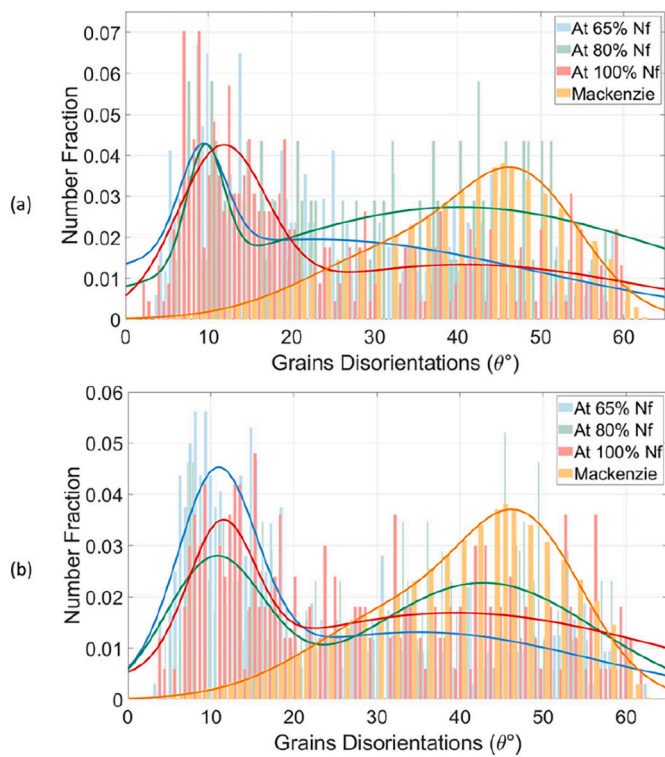


Fig. 12. Disorientation angles' evolution in the partitioned wire positions in chip #6 at the (a) tip & (b) heel.

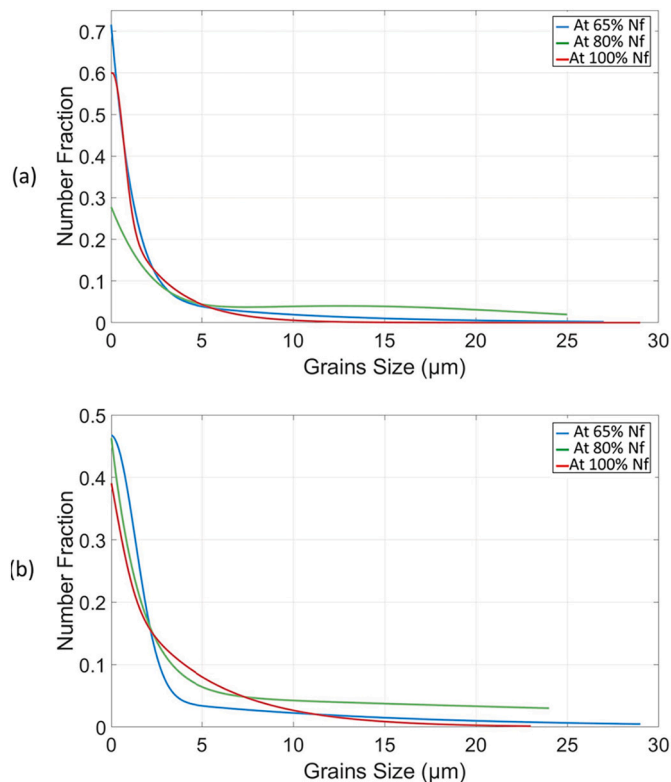


Fig. 13. Grain size's evolution for the partitioned wire positions in chip #6 at the (a) tip & (b) heel.

because cracks had already formed and stress was relieved. Recrystallization dominance justifies the high fraction of tiny grains. LABs are dominant as well at this stage, with the existence of some HABs.

After cycling to 80 % N_f , the volume fraction of recrystallization components highly decreased, accompanied by the generation of some deformation components. The increase in deformations is due to the fact that cracks themselves may induce deformations, especially at this advanced cycling stage. A shift from LABs to HABs is observed at this moment, simultaneously with the slowdown in the speed of the crack. Due to the previous recrystallization phase, grains had grown.

At 100 % N_f , the recrystallization component's volume fractions slightly increased, with a significant increase in deformations caused by cracks at this lifting-off moment. Such an increase in deformation and recrystallization components justifies the dominance of small grains.

3.2.4. Analysis at the heel position (65 % & 100 % N_f)

When looking at the heel position, it can be deduced that recrystallization components dominate at 65 % N_f . Deformation components exist with low volume fractions since cracks are already formed. Grains are mostly small, with the presence of some big sizes. LABs dominate at this moment as well.

Recrystallization components are still dominant when the sample is cycled up to 80 % N_f , even though their number fractions had decreased. This decrease is probably because most of the grains had been recrystallized. In addition, a shift from LABs to HABs is clear at this stage, at the same time as the crack speed slows down. Grains are bigger than before due to grain growth following recrystallization.

Finally, upon reaching the moment of complete failure, deformation components increased and became dominant over recrystallization textures which highly decreased, possibly due to the effect of cracks in generating stress, especially since we arrived at the lifting-off moment. The increase in deformations and the presence of a previous recrystallization phase are probably the reasons for the decrease in grains size through the generation of some sub-grains.

4. Interpretation of the crack evolution

Primarily, due to the wire welding process, deformations are created at the metallic contact sites, especially at the wire extremities, resulting in initial defects. Stress concentrates there upon cycling as well. Grains near the wire-metallization contact are small due to the welding forces ($<5 \mu\text{m}$), with a majority of LABs. A few HABs exist as seen in Fig. 14; such sites are preferable for crack nucleation than LABs. The reason is that HABs are considered as obstacles to dislocations migration, leading to their accumulation [19]. This increases the stress concentration and causes crack initiation. From Fig. 2, it is confirmed that cracks initiate from the wire contact ends, where some HABs exist (as seen in Fig. 14) with a faster speed at the heel position than at the tip.

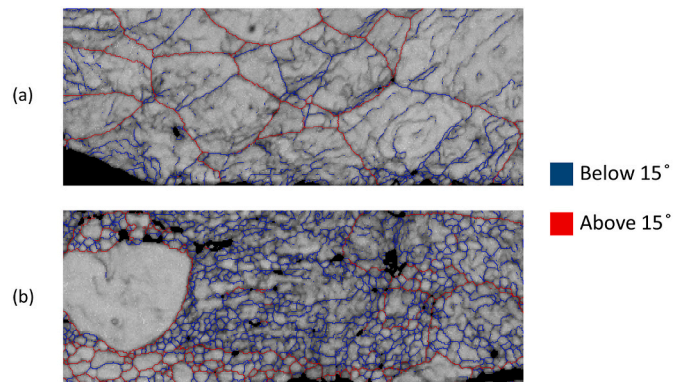


Fig. 14. Disorientation angles' distribution in the healthy sample (a) at the tip position and (b) at the heel position.

Cracks continue propagating from both edges toward the center of the bottom wire zone, as seen in Fig. 2. According to Fig. 14, LABs exist in crack propagation sites inside the wire just above the metallization. This is because the crack propagation is much easier to occur through LABs, due to their poor sliding and the ease of crack penetration. In Fig. 9, the highest crack speed at 10 % N_f is deduced to be concurrent with the increased number of LABs. Additionally, from Fig. 5, it was deduced that the grain growth process accompanies the highest crack initiation speed. This is in agreement with the Hall-Petch relationship. Afterward, the crack propagation speed decreases at advanced cycling stages, as seen in Fig. 2. This crack's slowdown was accompanied by an increase in the frequency of HABS at the interconnection sites, as seen in Figs. 6 and 12. Maybe this is due to the role of HABS in resisting crack propagation. Finally, when N_f is reached, cracks become completely distributed at the entire bottom wire zone, where lift-off occurs.

5. Conclusions

Since cracks propagate inside the wire just above the metallization in SKIM63 IGBT modules, this zone was analyzed. Grain's texture changes were shown to be driven by their stability by decreasing the surface energy. The evolution of texture components was then interpreted during cycling since they indicate whether deformations dominate or recrystallization. The relation between grains size and disorientation angles' evolution from one side, and the crack speed from the other was then discussed. Finally, the cracking scenario was detailed by relating its evolution to the microstructural changes.

CRedit authorship contribution statement

Mustafa Shqair: Conceptualization, Methodology, Software, Writing - Original draft preparation. **Zoubir Khafir:** Supervision, Conceptualization, Validation, Writing - Review & editing. **Ali Ibrahim:** Supervision, Conceptualization, Writing - Review & editing. **Ayda Halouani:** Writing - Review & editing. **Mounira Berkani:** Writing - Review & editing.

Declaration of competing interest

The authors declare that they have no known competing financial interests or personal relationships that could have appeared to influence

the work reported in this paper.

References

- [1] K. Kanert, R. Pufal, O. Wittler, R. Dudek, M. Bouazza, Modelling of metal degradation in power devices under active cycling conditions, in: 12th Intl.Conf. on Thermal, Mechanical & Multi-Physics Simulation and Experiments in Microelectronics and Microsystems, 2011, pp. 1–6.
- [2] R. Ruffilli, M. Berkani, P. Dupuy, S. Lefebvre, Y. Weber, Aluminum metallization and wire bonding aging in power MOSFET modules, in: Materials Today: Proceedings, 2018, pp. 14641–14651.
- [3] M.S. Broll, U. Geissler, J. Höfer, S. Schmitz, O. Wittler, K.D. Lang, Microstructural evolution of ultrasonic-bonded aluminum wires, *Microelectron. Reliab.* 55 (2015) 961–968.
- [4] J. Onuki, M. Koizumi, M. Suwa, Reliability of thick Al wire bonds in IGBT modules for traction motor drives, *IEEE Trans. Adv. Packag.* 23 (2000) 108–112.
- [5] N. Dornic, A. Ibrahim, Z. Khafir, N. Degrenne, S. Mollov, D. Ingrassio, Analysis of the aging mechanism occurring at the bond-wire contact of IGBT power devices during power cycling, *Microelectron. Reliab.* 114 (2020), 113873.
- [6] S. Häuser, in: SKIM® 63/93 Technical Explanations, 2013, pp. 1–43, no. October.
- [7] B. Beausir, J.-J. Fundenberger, Analysis Tools for Electron And X-ray diffraction, ATEX-software, Université de Lorraine, Metz, 2017.
- [8] W. Loh, M. Corfield, H. Lu, S. Hogg, T. Tilford, C.M. Johnson, Wire bond reliability for power electronic modules - effect of bonding temperature, in: International Conference on Thermal, Mechanical And Multi-physics Simulation Experiments in Microelectronics And Micro-systems, 2007, p. 6.
- [9] R. Tran, et al., Surface energies of elemental crystals, *Sci. Data* 3 (2016) 1–13.
- [10] A. Patra, J.E. Bates, J. Sun, J.P. Perdew, Properties of real metallic surfaces: effects of density functional semilocality and van der Waals nonlocality, *Proc. Natl. Acad. Sci. U. S. A.* 114 (2017) E9188–E9196.
- [11] J.M. Zhang, F. Ma, K.W. Xu, Calculation of the surface energy of FCC metals with modified embedded-atom method, *Appl. Surf. Sci.* 229 (2004) 34–42.
- [12] J.W. Wyrzykowski, M.W. Grabski, The Hall-Petch relation in aluminium and its dependence on the grain boundary structure, *Philos. Mag. A Phys. Condens. Matter Struct. Defects Mech. Prop.* 53 (1986) 505–520.
- [13] J.K. Mackenzie, Second paper on statistics associated with the random disorientation of cubes, *Biometrika* 45 (1958) 229–240.
- [14] D. Liu, D.J. Pons, Crack propagation mechanisms for creep fatigue: a consolidated explanation of fundamental behaviours from initiation to failure, *Metals (Basel)* 8 (2018) 623.
- [15] J. Lin, Y. Liu, T.A. Dean, A review on damage mechanisms, models and calibration methods under various deformation conditions, *Int. J. Damage Mech.* 14 (2005) 299–319.
- [16] J. De Paula Martins, A.L.M. De Carvalho, A.F. Padilha, Texture analysis of cold rolled and annealed aluminum alloy produced by twin-roll casting, *Mater. Res.* 15 (2012) 97–102.
- [17] D. Nyung, H. Nam, Recrystallization textures of metals and alloys, in: Recent Developments in the Study of Recrystallization, 2013, pp. 3–59.
- [18] Y. Zhou, L.S. Tóth, K.W. Neale, On the stability of the ideal orientations of rolling textures for F.C.C. polycrystals, *Acta Metall. Mater.* 40 (1992) 3179–3193.
- [19] M.D. Sangid, H.J. Maier, H. Sehitoglu, The role of grain boundaries on fatigue crack initiation - an energy approach, *Int. J. Plast.* 27 (2011) 801–821.